https://doi.org/10.5194/soil-2020-33
Preprint. Discussion started: 15 June 2020

Comparison of soil characteristics from geophysical and geochemical techniques along a climate and ecological gradient, Chilean Coastal Cordillera (26° to 38° S)

Mirjam Schaller[1*]

Igor Dal Bo[2*]

Todd A. Ehlers[1]

Anja Klotzsche[2]

Reinhard Drews[1]

Juan Pablo Fuentes Espoz[3]

Jan van der Kruk[2]

[1] Department of Geosciences, University of Tübingen, Germany, Schnarrenbergstrasse 94-96, 72076 Tübingen, Germany

[2] Agrosphere (IBG-3), Institute of Bio- and Geosciences, Forschungszentrum Jülich, 52428, Jülich, Germany

[3] University of Chile, Department of Silviculture and Nature Conservation, Av. Santa Rosa 11315, La Pintana, Santiago RM, Chile

* Authors contributed equally.

Corresponding author: E-mail: Mirjam Schaller (mirjam.schaller@uni-tuebingen.de)

https://doi.org/10.5194/soil-2020-33
Preprint. Discussion started: 15 June 2020

Abstract

In this study, we combine geophysical observations from Ground Penetrating Radar (GPR) with soil physical, and geochemical properties from pedons excavated in four study areas spanning 1,300 km of the climate and ecological gradient in the Chilean Coastal Cordillera. Our aims are to: (1) relate GPR observations to depth varying soil physical and weathering-related chemical properties in adjacent pedons, and (2) evaluate the lateral extent to which these properties can be extrapolated along a hillslope using GPR observations. Physical observations considered include soil bulk density and grain size distribution whereas chemical observations are based on major and trace element analysis. Results indicate that visually-determined soil thickness and the transition from the soil B to C horizons generally correlate with maximums in the 500 and 1000 MHz GPR envelope profiles. To a lesser degree, these maximums in the GPR envelope profiles agree with maximums in weathering related indices such as the Chemical Index of Alteration (CIA) and the chemical index of mass transfer (τ) for Na. Finally, we find that up-scaling from the pedon to hillslope scale is possible with geophysical methods for certain pedon properties available. Taken together, these findings suggest that the GPR profiles along hillslopes can be used to infer lateral thickness variations in soil horizons, and to some degree the physical and chemical variations with depth.

Keywords: soil, saprolite, hillslope, climate, vegetation, geophysics

https://doi.org/10.5194/soil-2020-33
Preprint. Discussion started: 15 June 2020

1 Introduction

Weathering of bedrock by biotic and abiotic processes produces regolith which provides resources for life. Most biota ~~is~~ found in an upper mobile layer (soil), which is underlain by an immobile layer of weathered material (saprolite) that replenishes the soil with nutrients through chemical weathering and erosion that drives nutrient uplift towards the surface (e.g., Porder et al., 2007). The ~~thickness and production~~ of ~~soil~~ is influenced by topography, tectonically driven rock uplift, climate, biota, composition (mineral content), and time (e.g., Hilgard, 1914; Jenny, 1994). However, sub-surface variations in soil thickness at the scale of hillslopes are difficult to quantify because of lack of exposure. Thus, subsurface imaging by geophysical techniques, when calibrated to soil pit excavations (pedons), offers ~~one~~ potential ~~mean~~ to characterize spatial variability in soil thickness and soil properties (e.g., Mellett, 1995; Doolittle and Collins, 1995; Miller et al., 2004). Here, we evaluate the utility of applying Ground Penetrating Radar (GPR) to map variations in soil properties in diverse climate and ecological settings with stark differences in physical and chemical soil properties.

Previous work has attributed spatial variations in soil thickness to hillslope curvature (Heimsath et al., 1997; Heimsath et al., 1999), which determines the downslope rate of mass transport assuming a diffusion based geomorphic transport law (e.g., Roering et al., 2001). However, this single point information is spatially restricted and pedon excavations are time-intensive. To further understand spatial variations in ~~soil and saprolite~~ thickness, other approaches such as modeling (e.g., Scarpone et al., 2016) and geophysical ~~imagining~~ (e.g., see summary in Parsekian et al., 2015) have been applied. For example, soil thickness variations were extrapolated from Digital Elevation Models (DEMs) in combination with several different observations at single locations (e.g., Scarpone et al., 2016). Different geophysical techniques have provided a non-or minimally invasive approach to view ~~soil variations~~ down to the ~~saprolite and~~ bedrock interface (e.g., Parsekian et al., 2015). Whereas high frequency GPR has proven suitable for investigating soil layering and thickness (e.g., Doolittle et al., 2007; Gerber et al., 2010; Roering et

https://doi.org/10.5194/soil-2020-33
Preprint. Discussion started: 15 June 2020

al., 2010; Dal Bo et al., 2019), other methods such as ~~seismics~~ (e.g., Holbrook et al., 2014), Electrical Resistivity Tomography (ERT, e.g., Braun et al., 2009), and low frequency GPR (e.g., Aranha et al., 2002) are better suited to image ~~saprolite and bedrock interfaces~~ (e.g., Parsekian et al., 2015). GPR methods were previously also used to indirectly measure ~~the distribution of~~ water flow (e.g., Zhang et al., 2014; Guo et al., 2020) as well as root density (e.g., Hruska et al., 1999; Guo et al., 2013). Interpreting the interplay of GPR signals with physical and chemical ~~soil~~ properties ~~within the sub surface~~ is challenging and not well-understood (e.g., Saarenketo, 1999; Sucre et al., 2011; Tosti et al., 2013; Sarkar et al., 2019).

The Chilean Coastal Cordillera (Fig. 1) contains an extreme climate and vegetation gradient and ~~it~~ is a natural laboratory to study the influence of climate and vegetation on ~~the sub surface of the Earth~~ in a setting with a similar tectonic history and lithology. The region is home to four study areas of the German-Chilean EarthShape priority program (www.earthshape.net), where investigations of biotic interactions with critical zone processes are conducted (e.g., Bernhard et al., 2018; Oeser et al., 2018). The study areas were selected due to the arid climate in the northernmost location (26° S), and temperate rain forest conditions in the southernmost location (38° S). These four study areas are investigated to both qualitatively and quantitatively describe the differences between the four settings. Our previous work in these areas has so far identified increases in soil thickness from north to south and major and trace element compositional variations within pedons (e.g., Bernhard et al., 2018; Oeser et al., 2018; Dal Bo et al., 2019). However, a detailed comparison of geophysical, geochemical, and soil observations is yet to be conducted in these areas.

In this ~~study~~, we investigate how physical as well as chemical ~~observations~~ measured at point locations (pedons) relate to GPR observations to gain further insight into ~~the~~ sub-surface variations. In general, we find that GPR signals can be correlated to changes in soil physical properties if these changes are of sufficient magnitude and laterally coherent. If such a correlation is observed, we discuss the links between the physical and chemical properties. The comparison of physical and

https://doi.org/10.5194/soil-2020-33
Preprint. Discussion started: 15 June 2020

chemical properties with field observations and GPR data helps to better understand the sub-surface at point locations (e.g., soil thickness) and in some cases allows for up-scaling point observations to the hillslope scale along a GPR measurement profile.

2 Study areas

Four primary study areas are investigated ~~in~~ the climatic and vegetation gradient observed in the Chilean Coastal Cordillera (Fig. 1 and 2; Table 2). From N to S, the four selected areas are: a) Pan de Azúcar (~26.1° S); b) Santa Gracia (~29.8° S); c) La Campana (~33.0° S); and d) Nahuelbuta (~37.8° S).

2.1 General climate, vegetation, and geologic setting

The Chilean Coastal Cordillera with its climate and vegetation gradient is a natural laboratory to study the influence of climate and vegetation on denudation (Fig. 1). From N to S (~26° to 38° S), present climate ranges from arid to humid-temperate. The mean annual precipitation increases from close to zero to ~1500 mm yr^{-1}, and mean annual temperature decreases from ~20° C to ~5° C. The flora consists of small shrubs, geophytes and annual plants (Armesto et al., 1993) in the N and changes to lower-stature deciduous trees and shrubs ~~intermix~~ with tall evergreen mixed forest in the S. Vegetation cover increases from close to zero to ~100%.

Climate and vegetation in the primary study areas changed over time from the Last Glacial Maximum (LGM) to present. Mean annual precipitation during the LGM was higher than at present in all four study areas (Mutz et al., 2018). Mean annual temperature during the LGM was lower than at present except in the southernmost study area where mean annual temperature stayed the same (Mutz et al., 2018). Hence, the climate gradient observed today is comparable to the gradient during the LGM. Even though the climate was wetter and cooler during the LGM, no glaciers covered any of the study areas (Rabassa and Clapperton, 1990). ~~Due to~~ these

https://doi.org/10.5194/soil-2020-33
Preprint. Discussion started: 15 June 2020

climatic changes over time, vegetation zones during the LGM were shifted northward by ~5° and vegetation cover was slightly (~5-10%) lower compared to present (Werner et al., 2018). This shift of vegetation zones to the N and the decrease in vegetation cover also likely influenced the fauna present, but to an unknown degree.

To compare the effect of climate and vegetation on soil thickness and GPR observations, differences in lithologies need to be minimal. However, these conditions are not always fulfilled and need to be taken in to account. Whereas bedrocks in Pan de Azúcar, La Campana, and Nahuelbuta are granites to granodiorites, the bedrocks in Santa Gracia range from Granodiorites to Gabbros (Oeser et al., 2018). Hence, the parent material in Santa Gracia is lower in the SiO_2-content (50-65%) in comparison to the other three study areas (SiO_2-content >65%). Chemical weathering and physical erosion may be affected by this difference, which in turn influences soil formation and thickness.

2.2 Soil Characteristics

In each study area, depth profiles from a catena consisting of three profiles on the S-facing slope (top-slope, mid-slope, and toe-slope) and one profile on the N-facing slope (mid-slope) were described, sampled, and analyzed (Fig. 3; see also Bernhard et al., 2018; Oeser et al., 2018; Schaller et al., 2018; Dal Bo et al., 2019).

Previous soil studies from pedons in each area identify O, A, B, and C horizons (e.g., Bernhard et al., 2018) that overlie weathered bedrock (e.g., Oeser et al., 2018). In this study, we follow the approach of Riebe and Granger (2013) and refer to depth profiles as regolith profiles that are composed of a mobile soil layer that includes the A and B horizons, and an immobile saprolite layer represented by the C horizon.

In Pan de Azúcar, the soil is part of a regosol and consists of a 20 to 25 cm thick A and B horizon. The total organic carbon content is <0.1% (Bernhard et la., 2018). The observed angular fragments in the soil increase in size (> 1 mm) with depth. The underlying saprolite is coarse-grained and jointed (Oeser et al., 2018). The

https://doi.org/10.5194/soil-2020-33
Preprint. Discussion started: 15 June 2020

average bulk density of the soil layer is 1.3 g cm^{-3}. The ~~cambisol in Santa Gracia consists of~~ 30 to 55 cm thick layers ~~of soil~~ with A and B horizons overlying the saprolite (Bernhard et al., 2018). The total organic carbon content is 0.4%. Whereas the A horizon consists of a silt- to fine sand-sized matrix supporting up to 2 mm sized fragments, the underlying B horizon shows a transitional increase of fragments to a coarse fragment-supported fine-grained matrix (Oeser et al., 2018). The average bulk density is 1.5 g cm^{-3}. The soils ~~and saprolites~~ in La Campana ~~form~~ a cambisol. The soil layers consisting of A and B horizons are 35 to 60 cm thick and have a total organic carbon content of 1.9% (Bernhard et ~~la~~., 2018). The fine sand- to silt-sized A horizon contains fragments of up to 3 mm. The matrix in the underlying B horizon is coarsening downwards and the number of fragments increases such that the horizon shifts from matrix- to clast-supported. The average bulk density is 1.3 g cm^{-3}. The ~~umbrisol in Nahuelbuta consists~~ of a 60 to 90 cm thick ~~soil~~ layer (A and B horizons) and a readily disaggregating saprolite. The total organic carbon content in these soils is 6.1% (Bernhard et la., 2018). The A horizon is composed of silt-sized particles forming nodular soil aggregates. In the upper part there are up to 1 mm large quartz grains embedded whereas the lower part contains large fragments. The fine sand-sized matrix of the transitional B horizon hosts subangular fragments. The amount and size of these fragments increases with depth. The average bulk density of the soil layer is 0.8 g cm^{-3}.

3 Data compilation and methods

New data from 32 GPR profiles in the four study areas were collected at frequencies of 500 and 1000 MHz. These data are compared to physical and chemical properties from point locations (pedons) from previous studies (Bernhard et al., 2018; Oeser et al., 2018). These new GPR profiles complement previous GPR data collected at the same frequencies~~,~~ in the same catchments (Dal Bo et al., 2019). The difference between this study and that of Dal Bo et al. (2019) lies in the

https://doi.org/10.5194/soil-2020-33
Preprint. Discussion started: 15 June 2020

new, more extensive, GPR data coverage and the comparison of it to physical and chemical subsurface variations.

Using chemical and physical properties collected in pedons to understand the corresponding radar signatures is a difficult task requiring treatment on multiple layers. First, it would need fixed relationships translating the measured pedon properties to corresponding permittivity changes relevant for the radar signal. Second, it would need a radar forward model that successfully predicts the convolution of the emitted radar pulse with the sub-surface reflectivity. This includes among others handling constructive and destructive interference caused by closely-spaced permittivity changes in the vertical. For applications on soil, this is currently not possible because already the permittivity relationships are unclear. We therefore take a step back from the more sophisticated methods, and use simpler statistical metrics trying to isolate some properties (i.e. Pearson correlation) or combinations thereof (i.e. Principal Component Analysis) that may explain parts of the radar signatures.

3.1 Data compilation

In this ~~study,~~ GPR data are compared to previously published soil and saprolite physical and chemical properties (Table 1) such as: 1) soil bulk density, grain size distribution, pH, and cation exchange capacity - CEC (Bernhard et al., 2018); and 2) Loss On Ignition - LOI, Chemical index of Alteration - CIA, mass transfer coefficient τ, and volumetric strain, ε_{strain} (Oeser et al., 2018). The grain size distributions provide a measure of the weight percent of different grain sizes smaller than 2 mm in the regolith, and the regolith bulk density provides a measure of how dense the soil and saprolite material is packed. The geochemical data used provide major and trace element analysis, the acid and base properties (pH) and cation exchange capacity (CEC). Major and trace element analysis allow the investigation of the loss on ignition (LOI), the chemical index of the mass transfer coefficient (τ), and the volumetric strain (ε_{strain}). LOI is a measure of the loss of volatile substances in a material due to excess heating (1000°C), thereby reflecting the amount of soil

https://doi.org/10.5194/soil-2020-33
Preprint. Discussion started: 15 June 2020

organic matter. The degree of weathering can be quantified by the CIA which is sensitive to the removal of alkalis such as calcium, sodium, and potassium from feldspars (Nesbiitt and Young, 1982). The mass transfer coefficient (τ_{strain}) reflects chemical gains and losses during weathering based on the elemental concentrations of mobile and immobile elements in weathered and unweathered material (e.g., Brimhall et al., 1985; Chadwick et al., 1990), ε in a regolith is based on the density ρ (g cm^{-3}) and immobile element concentrations of the weathered regolith in comparison to the unweathered bedrock indicating volumetric gain or loss (Brimhall and Dietrich, 1987).

3.2 Ground Penetrating Radar (GPR)

Ground Penetrating Radar (GPR) is a geophysical technique based on the emission of pulsed electromagnetic waves into the subsurface and here frequencies of 500 and 1000 MHz are applied. The electromagnetic waves are reflected and scattered in the presence of dielectric contrasts at depth. The back-propagated reflected wave is then received at travel times, which depend on the depth-variable electromagnetic wave velocity *v.* The velocity of the media is dictated by the relative dielectric permittivity ε_r (Jol, 2009). The attenuation of the waves can be linked to the electrical conductivity σ. The vertical resolution depends on the system's bandwidth and the wave velocity and is in our case approximately 0.07 m for 500 MHz and 0.03 m for 1000 MHz. Surface GPR can be measured in two ways including: 1) Common-Offset Profiling (COP) and 2) Common-midpoint (CMP) or wide-angle-reflection-refractions (WARR) measurements (see also Dal Bo et al., 2019). COPs measure traveltime versus spatial position along specific transects with two antennae at fixed offsets. Here, this was done along profiles crossing the pedons (e.g., Fig. 2 and 3). WARRs are used to retrieve velocity and physical properties at the point scale with variable antennae spacing. Specifically, for each pedon a WARR was measured in a relatively flat location by keeping the transmitter position fixed at the pedon location and by moving the receiver towards the transmitter with a step size varying between 0.01 and 0.05 m depending on the

https://doi.org/10.5194/soil-2020-33
Preprint. Discussion started: 15 June 2020

deployed frequency. In such way, the move-outs of linear events (air wave and ground wave) and of hyperbolic events (sub-surface reflections) could be identified using the underlying assumption that internal reflectors are not dipping.

Twenty-eight COP transects going from hillslope toe (near valley) to top (ridge crest) were collected in the four study areas using 500 and 1000 MHz GPR antennae (Sensor and Software Inc.). The average trace spacing of these vary between 0.01 and 0.05 m depending on frequency and location. These transects were chosen in such a way as to run between pedons, where the previously described physical and chemical properties were collected (Bernhard et al., 2018; Oeser et al., 2018). Of these 28 profiles, two were collected in the Pan de Azúcar study area, six in Santa Gracia, three in La Campana, and three in Nahuelbuta. Each profile was measured twice to total 28 (at the two frequencies). The pedon locations formed the basis for comparison to the GPR data as ground-truth data and WARRs and COPs where collected specifically at these positions (red stars, Fig. 2). Additionally, four perpendicular GPR crosslines (perpendicular to the transects) were measured at both the 500 and 1000 MHz in the La Campana and Nahuelbuta study areas. The position of each profile was determined using a differential GPS (Leica Geosystems AG) with a maximum horizontal and vertical precisions of 2 and 4 cm, respectively.

GPR data were processed and analyzed similar to Dal Bo et al. (2019) using MATLAB. The GPR data processing procedure included: frequency band-pass filter, amplitude gain, background removal, and time-to-depth conversion (e.g., Jol, 2009). The direct air wave between receiver and transmitter was muted. Similar to Dal Bo et al. (2019), the newly measured WARR profiles at the pedon locations were processed and analyzed using a combined linear move-out – hyperbolic move-out approach. Ground wave and reflection velocities were picked, from which an average value of GPR velocity per each study area was derived and used for the time-to-depth conversion of the COP profiles (see Dal Bo et al., 2019). The averaged value of GPR velocities is used to study soil depths on hillslope scale. However, the use of an average will result in an over-/under-estimate of soil depths on the hillslope scale. Signal envelopes were calculated using a Hilbert transform (Green, 2004; Liu and Marfurt, 2007). At each pedon location, a certain number of traces depending on the measurement step size (i.e. between 10 and 50) were sampled for 0.5 m uphill and 0.5 m downhill the pedon and laterally averaged for comparison to the pedon physical and chemical properties. The averaging assumes that both chemical and GPR signatures do not change with depth across that interval, an assumption that may not hold everywhere. As the GPR envelope is directly related to the electric impedance (Telford et al., 1990; Jol, 2009), the envelope onset and energy intervals could be compared to variations in physical, and potentially chemical, soil properties.

3.3 Statistical Correlation and Principal Component Analysis

Comparison between the chemical and physical pedon information (Bernhard et al., 2018; Oeser et al., 2018) and GPR data was conducted two different ways. First, we carried out a correlation analysis using the Pearson' correlation coefficient (*r*). More specifically, we used the bulk density, clay content, LOI, CIA, Tau (τ), volumetric strain (ε_{strain}), pH, and CEC for comparison to the GPR 500 and 1000 MHz antennae envelope data. The GPR envelopes were resampled and averaged, such that the depth intervals were the same as for the derivates of the soil data (see Table S2). Furthermore, because the envelope of GPR data is sensitive to changes along the vertical direction, we also calculated the vertical gradient of the ground truth information at each sampled depth using a centered difference approximation. Following this, the R package function corrplot (Wei, 2012) was used to calculate the Pearson's correlation coefficient to identify correlations between the variables (Sedgwick, 2012). This analysis was done considering the entire climate and vegetation gradient and within each location. Both the original data and the derivatives were used to explore which of the two approaches delivered meaningful insights.

Second, we conducted a multivariate analysis of the data using a principal component analysis (PCA; Wold et al., 1987). This was done for both the entire

https://doi.org/10.5194/soil-2020-33
Preprint. Discussion started: 15 June 2020

climate gradient and within each study area using the factoextra R package (Kassambara, 2017). After each PCA analysis, a scree plot was evaluated to investigate how much variance was included in each principal component (PC, Bro and Smilde, 2014). In this study, at least 70% of the variance was among the first two PCs, which were then further analyzed. The contribution of each variable to the first and second PC was computed using the eigenvalues and eigenvectors from the covariance matrix (Abdi and Williams, 2010). This resulted in a plot where the x-axis is PC1 and the y-axis is PC2 and each variable is displayed as a vector with a specific direction and length that indicate the magnitude and direction of the contribution to each PC.

4 Results

Physical and chemical properties from pedons are shown with the 500 and 1000 MHz GPR profiles and their envelopes with depth as well as investigated correlations and PCAs for the four study areas (Fig. 4 to 11 and supplement Figs S1 to S12; and supplement Tables S1A to D, S2A to D, S3, and S4A to E). For brevity, only the comparisons between pedon observations and GPR data are presented for the S-facing mid-slope positions in the main text (Fig. 4, 6, 8, and 10) and the remaining locations are provided in the supplementary material. Note that the envelopes are averaged over the COP data, collected over a lateral distance of 1 m in total, and are therefore not point information. Given that the soil thickness increases towards the southern study areas, the 1000 MHz GPR antennae is interpreted for the (northern two) Pan de Azúcar and Santa Gracia study areas, whereas in La Campana and Nahuelbuta the 500 MHz GPR signal was used because it has a deeper penetration depth. However, we show results below for both frequency antennas to demonstrate the difference in penetration depth and resolution between the two antennae. Details for each study area (from N to S) follow.

https://doi.org/10.5194/soil-2020-33
Preprint. Discussion started: 15 June 2020

4.1 Pan de Azúcar (northern most study area)

In Pan de Azúcar (Fig.1, 2A), a gradual transition from the B to the C horizon was visually observed in the pedons at 20 to 40 cm whereas the mobile/immobile boundary is considered to be at 20 to 25 cm (shaded gray areas and black line, Fig. 4, Fig. S1 to S3). The available physical properties for this location do not indicate a strong change in material properties with depth. LOI and CIA indicate a minor change in properties at ~20 cm depth. A maximum in the energy envelope in the 1000 MHz frequency is present at about 20 to 30 cm that could be related to the transition of material properties between the B and C horizons and the location of mobile/immobile boundary observed in the field.

Due to the sparse depth information for bulk density and clay content, the statistical analyses for this location was not very insightful. Whereas clay content shows a medium correlation (0.54) with the 1000 MHz GPR envelope, no strong correlation between LOI, CIA, τ, and the 1000 MHz GPR envelope could be found (Table S3). In the PCA, three primary components (PC) explain over 80% of the variance (Table S4A). PC1 has the bigger contribution from CIA, clay content, and the 500 MHz envelope whereas PC2 has the bigger contribution from LOI, the 1000MHz envelope, and τ of Na and Zr (Fig. 5).

4.2 Santa Gracia

In Santa Gracia (Fig. 1, 2B), a gradual transition from the B to the C horizon was observed in the field between 20 to 60 cm depth (shaded gray region Fig. 6, Fig. S4 to S6). The boundaries between the mobile/immobile layers in the pedon were observed between 30 to 55 cm depth. Bulk density and volumetric strain show slight changes around 15 and 30 cm depth. Whereas LOI and CIA do not show any changes with depth, τ shows changes between 30 and 50 cm depth. The 500 and 1000 MHz GPR profiles and envelopes show increased irregular and strong reflections at ~25 cm (1000 MHz) and 45 cm (500 MHz) depth, and also maximums in the envelope at ~25 cm (1000 MHz) and 45 cm (500 MHz) depths. These

https://doi.org/10.5194/soil-2020-33
Preprint. Discussion started: 15 June 2020

variations in the reflections and maximums in the envelopes coincide with either the top or central position of the transition from the B to the C horizon.

A weak to moderate correlation (~0.3) between clay content as well as CIA and the 1000 MHz GPR envelope is present (Table S3). Results from a PCA analysis of the Santa Gracia data indicate that 3 components explain over 80% of the observed variance (Table S4B). PC1 explains over 35% of the variance, and includes bulk density, CIA, and the 500 and 1000 MHz envelopes (Fig. 7). PC2, explaining 31% of the variance, includes clay content, LOI, and τ of Na and Zr.

4.3 La Campana

Field observations from the La Campana area (Fig. 1, 2C) document a layer of cobbles (5 to 10 cm diameter) between the A and B horizon at a depth of ~30 cm (Bernhard et al., 2018). The transition between the B to C horizons does not contain rock fragments. The transition from the B to C horizon (shaded gray area, Fig. 8) and the mobile/immobile boundary (black line, Fig. 8) are observed at 34 to 110 cm and 35 to 60 cm, respectively (see also Fig. S7 to S9). The mobile soil layer extends deeper in La Campana than in Pan de Azúcar or Santa Gracia and physical properties were available for greater depths. Bulk density and grain size change gradually with depth and no soil thickness could be determined. Also, LOI, CIA, and τ do not show an abrupt change in regolith properties. Reflection hyperbolas and irregular reflection horizons appear in the 500 and 1000 MHz GPR data at about 40 to 60 cm depth above the B to C horizon transition. The second peaks of the 500 and 1000 MHz GPR envelopes coincide with the B to C horizon transition.

In contrast to the previous study areas, the 500 MHz GPR envelope correlates moderately with CIA (0.56), pH (-0.57), and CEC (-0.39, Table S3). Three components from the PCA analysis explain about 80% of the total variance (Table S4C). PC1 (~35% of the total variance) includes LOI, τ, and CEC, whereas PC2 (31%) contains CIA, volumetric strain, and the envelopes (Fig. 9). PC3 is dominated by pH as well as τ of Zr. In general, whereas the first energy interval (1000 MHz)

https://doi.org/10.5194/soil-2020-33
Preprint. Discussion started: 15 June 2020

could be attributed to the stone layer between the A and B horizon, the second energy interval occurs close to (<10 cm) with the mobile/immobile boundary (Fig. 8).

4.4 Nahuelbuta (southernmost study area)

In Nahuelbuta, the B horizon contains pebbles and cobbles at around 60 to 80 cm depth (Bernhard et al., 2018). The B to C horizon transition appears at 50 to 100 cm depth (shaded gray region, Fig. 10; see also Fig. S10 to S12). The mobile/immobile boundary was identified at 60 to 90 cm depth. Density measurements in the pedon indicate a transition in bulk density between about 30 to 60 cm depth where also the grain size distribution changes. The LOI and τ generally show large changes with depth, in contrast to the CIA and volumetric strain which are more homogenous with depth. The 500 MHz GPR profile indicate the existence of point targets/objects appearing as reflection hyperbola or undulating features at depths greater than 60cm. This depth is approximately the same depth at which the mobile/immobile boundary was identified, as well as changes in the physical (e.g. bulk density, percent sand) and chemical (LOI, τ) properties. The hyperbolas do not add up coherently during the lateral averaging and therefore do not produce a significant energy interval in the average envelope. The envelope is dominated by the energy intervals given by two reflections at about 30 to 50 cm depth. The lower set of these energy intervals could be linked with the upper physical soil boundary.

Results from the correlation analysis indicate the 500 MHZ GPR envelope is strongly positively correlated with bulk density (0.74), strongly inversely correlated with LOI (-0.6), and moderately inversely or positively correlated with clay content (-0.37), pH (0.46), and CEC (-0.53) (Table S3). Results from the PCA analysis show that two PC components explain ~75% of the variance. PC1 (~57 %) includes bulk density, clay content, LOI, and CEC, whereas PC2 (~18 %) contains τ of Zr and pH (Fig. 11; Table S4D). In general, as the 500 MHz GPR envelope signal correlates

https://doi.org/10.5194/soil-2020-33
Preprint. Discussion started: 15 June 2020

well with bulk density and clay content, the envelope signal reflects changes in soil properties.

5 Discussion

Here we evaluate the chemical, physical, and geophysical observations from the pedons. Using this information, we attempt to up-scale information from the pedons to the hillslopes scale along the GPR transects. Potential soil thickness over hillslopes is discussed in light of hillslope, aspect, and the climate and vegetation gradient from N to S.

5.1 Synthesis of GPR data with physical and chemical properties from point locations

GPR data image changes in material properties that could be caused by changes in physical (e.g., bulk density, grain size variation, water content), or potentially chemical properties (e.g., pH, CEC, CIA). The interplay between these different properties can have a complicated influence on the GPR signal and therefore difficult to disentangle. Disentangling any relationship between GPR data and physical and chemical properties is further complicated as not all properties influencing GPR data are measured (e.g., water content; Jol, 2009). In addition, the determination of soil thickness (i.e., the boundary between the mobile/immobile layers) in the field causes its own problems as observed changes are transitional over a depth interval of 5 to 10 cm and not discrete. In the following, we start by discussing if GPR data can be used to image soil thickness as well as physical and chemical properties at the pedon locations where *in-situ* observations were made in each study area.

In Pan de Azúcar (Fig. 4, 5 and Fig. S1 to S3), the locations where GPR data can be compared to pedons shows low variability in the observed soil thickness (~20 to 30 cm) at each pedon location. Whereas the 500 MHz signal shows deep (sub-soil depth) interfaces, the maximum in the 1000 MHz energy interval signal agrees

https://doi.org/10.5194/soil-2020-33
Preprint. Discussion started: 15 June 2020

with the soil thicknesses observed in the field (Fig. 4 and Fig. S1 to S3). However, the boundary between soil and saprolite layers is here probably too shallow to be detected with the 1000 MHz antennae. An even higher frequency would be favourable to detect the soil/saprolite boundary. Hence the Pearson correlations and PCA results from Pan de Azúcar are restricted not only because of GPR analysis but also due to restricted physical properties. The chemical and physical properties correlate only weakly to moderately with the 1000 MHz envelopes (Table S3). The PCA results indicate that soil bulk density is not likely correlated with either the 1000 MHz signal or LOI. In Pan de Azúcar, LOI does not represent soil organic matter as soils of the arid zones have low or no organic matter content. The volatile loss measured in the LOI is more likely associated with the combustion of carbonates. In general, shallow soils in the arid zone do not show much variability in soil thickness nor provide insight into the influence of physical or chemical properties on GPR signals.

In Santa Gracia (Fig. 6, 7 and Fig. S4 to S6), the field-observed soil thicknesses of the different pedons are more variable than in Pan de Azúcar. Although the 500 MHz and 1000 MHz GPR envelopes indicate changes at depth, the physical and chemical properties observed with depth show only a few distinct changes implying that the soil thickness cannot easily be determined using only physical or chemical properties. The PCA indicates that most of the variance in PC1 is explained by the envelope signals, bulk density, and CIA whereas PC2 is dominated by clay content and τ of Na and Zr. The clay content does not seem to be a dominant factor for the envelope signal, but rather represents a complex interaction between physical and chemical property changes that cannot be disentangled with available data. It appears that the second energy interval in the 1000 MHz envelope may agree with the observed soil thickness in Santa Gracia, and (in contrast to the Pan de Azúcar location) the first maximum in the 500 MHz envelope does agree with the observed soil thickness. These observations again underscore that for different locations with variable soil type, vegetation, and physical and chemical properties local calibration between pedons and GPR data are required.

https://doi.org/10.5194/soil-2020-33
Preprint. Discussion started: 15 June 2020

SOIL Discussions Open Access EGU

The determination of soil thickness from GPR data in La Campana is as difficult as in the previous settings (Fig. 8, 9 and Fig. S7 to S9). The field observations indicate relatively large transition zones for the B to the C horizon, and some physical properties vary only weakly with depth. As a result, the determination of soil thickness with physical and chemical properties is difficult, despite the moderate to strong correlation of 500 MHz GPR envelopes with derivatives of physical and chemical properties. Whereas the variance in PC1 is explained by bulk density, LOI, τ of Na and Zr, and volumetric strain, the variance in PC2 is dominated by the envelopes, CIA, pH, and CEC. Chemical properties seem to have a considerable influence on GPR signals in this setting. In La Campana, the first energy interval of the 500 MHz envelope is interpreted to reflect the previously described stone layer whereas the second energy interval seems to match the observed soil thickness. Given these uncertainties in local conditions, a clear identification of soil thickness from GPR data is difficult, even with local calibration to a pedon.

Finally, in Nahuelbuta (Fig. 10, 11 and Fig. S10 to S12), the observed soil thickness in the field is the deepest of all the four study areas and reaches from 50 to 100 cm. The soil thickness is easily identifiable based on physical properties. The derivatives of the physical properties correlate moderately with the available 500 MHz envelope (Table 3). Furthermore, the chemical properties correlate weakly with the GPR envelops. The variance is strongly explained by PC1 containing physical properties (e.g., bulk density, clay content, LOI) and less by PC2 including chemical properties (e.g., pH, τ of Na and Zr). Even so changes in properties are more pronounced in Nahuelbuta than in the drier locations, a clear correlation between maximums in the 500 MHz energy envelope and soil thickness is not present. The second energy interval of the 500 MHz envelope best agrees with the observed soil thickness. However, due to local inhomogeneities caused by intense vegetation, every pedon and its attributed GPR envelope look different.

In summary, the 500 and 1000 MHz envelopes at point locations have the potential to be used to determine soil thickness. But, the clarity with which this can be done is variable and requires calibration to local pedons. Even with local

https://doi.org/10.5194/soil-2020-33
Preprint. Discussion started: 15 June 2020

calibration, the relationships are not always clear (e.g., Fig. 8). Physical and chemical properties with depth exert a complex interplay on measured GPR signals. If a certain combination of physical and chemical properties is dominant in one setting, another combination may influence the measured GPR signal. Therefore, what GPR frequency works best for the individual study area due to different physical and chemical properties needs to be investigated with information from point locations/pedons. For the arid Pan de Azúcar and semi-arid Santa Gracia we suggest using the 1000 MHz frequency (or higher), whereas for the Mediterranean climate setting of La Campana and temperate Nahuelbuta the 500 MHz frequency proved better. Improvements in our approach to determine soil thickness from GPR data might be possible by applying multifrequency GPR techniques, which are freed from antenna effects by fusion of different frequency measurements (e.g., De Coster and Lambot, 2018). Nevertheless, the point information of soil thickness has the potential to be up-scaled to hillslopes in some settings using GPR transects after local calibration is conducted.

5.2 Up-scaling to hillslopes

Here we use insights gained from comparisons between GPR and point locations to extrapolate the soil thickness along the hillslope GPR profiles (Fig. 2, 3). The up-scaling is carried out using a combination of amplitude and envelope depth-converted profiles. To do this up-scaling, we calculated the envelope along each profile. Then, using the known soil depth data from all pedons in one study area, this interface was estimated along the profiles by searching for the corresponding signal in the envelope at every meter. Even though the information of three-point locations is at the lower limit, the combination of field observations with GPR transects allows estimation of the lateral variability of soil thickness over hillslopes. However, given the complications mentioned in section 5.1 (e.g., which frequency GPR antenna and envelope interval to use) the up-scaling and the indicated soil thickness need to be treated with care.

https://doi.org/10.5194/soil-2020-33
Preprint. Discussion started: 15 June 2020

In Pan de Azúcar (Fig. 12; Supplementary Fig. S14) the observed B to C horizon transition at point locations is typically between ~14 to 50 cm. No clear soil thickness could be determined based on GPR profiles. Nevertheless, soil thicknesses identified from 1000 MHz GPR envelopes seem to be relatively homogeneous over the entire S-facing transect with an average value of 25 ±3 cm (Table 2). In contrast, the N-facing transect indicates a thinner soil uphill than downhill where it reaches a maximum depth of ~50 cm (Fig. S14).

In Santa Gracia (Fig. 13; Supplementary Fig. S15 to 17), the soil thicknesses from point locations/pedons in the S-facing transect increases downslope and ranges between 20 to 60 cm (Table 2). The soil thickness based on the 1000 MHz GPR envelope at the top-slope position (SGPED20) decreases first downhill and then increases again, thereby demonstrating laterally variability along the hillslope. The soil thickness in the mid-slope position (SGPED40) is variable and reaches from 25 to 50 cm. At the toe-slope position (SGPED60) a mostly constant thickness of 30 cm is identified. In the N-facing transect almost no variability in soil thickness (~25 cm) is observed. Even so the soil thickness based on GPR envelopes cannot be used to decipher the exact soil thickness, the method still offers a close approximation of soil thicknesses determined by field observations and GPR profiles.

In La Campana (Fig. 14; Supplementary Fig. S18 to 20) the soil thickness from the 500 MHz GPR envelope is 35 to 70 cm. Whereas the top- and mid-slope positions in the S-facing hillslope (LCPED10 and LCPED20, respectively) show variable soil thickness between 50 and 70 cm, the toe-slope position (LCPED30) contains soil thicknesses between 35 and 70 cm. Relatively constant soil thickness of 50 to 60 cm are identified for the N-facing mid-slope position (LCPED40). Field observations do not always agree with soil thicknesses based on GPR envelopes. In the La Campana location, soil thicknesses based on GPR envelopes need to be considered with caution, but contain valuable information such as the existence of pebble layers. However, GPR profiles show hyperbolas and continuous reflections, which can be interpreted along almost all the covered length. These interfaces can

https://doi.org/10.5194/soil-2020-33
Preprint. Discussion started: 15 June 2020

be reliably used to infer soil thicknesses, when a previous calibration with soil pedons has been done.

In Nahuelbuta (Fig. 15; Supplementary Fig. S21 to 23), soil thickness in the S-facing top-slope position (NAPED10) increase downhill from 60 to 110 cm. At the mid-slope position (NAPED20), the soil thickness is highly variable and ranges from 50 to 110 cm. Soil thickness at the toe-slope position (NAPED30) is 80 to 110 cm. In the N-facing mid-slope position the soil thickness ranges from 60 to 110 cm. Soil thicknesses based on GPR envelopes are generally thicker than soil thicknesses observed in the field and ~~do also~~ not agree well with thicknesses based on GPR profiles. The application of GPR envelopes to determine soil thicknesses needs to be treated with care in this setting. On the contrary, GPR profiles display rather continuous reflections that might represent interfaces within the soil, and could therefore be used to extrapolate point-scale ground-truth information over the profile scale.

5.3 Changes of soil thickness with hillslope position, aspect, and latitude

The soil thickness imaged with GPR envelopes over hillslope transects reflect mainly physical properties, but also chemical properties (e.g., CIA, τ). This approach gives the opportunity to study non-invasively possible changes in soil thickness over hillslope position, aspect, and latitude (Fig. 12 to15; Fig. S14 to S24; Table 2). Here we summarize any regional trends in soil thickness between the four study areas and different aspect (N- vs. S-facing) hillslopes (Fig. 2).

Soil thickness in ~~a catena~~ that develop under comparable climate and on similar lithologies are expected to increase downhill (e.g., Birkeland, 1999). From the top- to toe-slope position along a catena the potential for physical erosion decreases downslope due to decreasing physical potential whereas the potential for deposition increases. In Pan de Azúcar, the soil thickness based on the GPR envelopes in the S-facing hillslope are constant, whereas the N-facing hillslope indicates soil thickness increasing from top- to toe-slope. The possible slight increase in soil thickness from top- to toe-slope can be explained by low denudation rates due to

https://doi.org/10.5194/soil-2020-33
Preprint. Discussion started: 15 June 2020

very low precipitation rates in Pan de Azúcar. In Santa Gracia, the constantly thin soils at the S-facing top-slope are in contrast to the thicker and more variable soil thickness in the mid-slope position. Bernhard et al., (2018) describe an increase of the A to BC horizon from top- to toe-slope in the S-facing hillslope. In Santa Gracia, precipitation and minor vegetation cover may cause the increase of the soil thickness downslope as well as the variable soil thickness in the mid-slope position. In La Campana, the soil thickness based on GPR envelopes is highly variable. Bernhard et al., (2018) observed the thickest soil also in the mid-slope position, describe a disturbed hillslope with recent erosion events (e.g., possibly due to a past fire and temporary mobilization of sediment). Therefore, the S-facing hillslope in La Campana is a disturbed system and therefore difficult to laterally extrapolate horizons. Due to the differences in soil thickness information from the different methods, soil thickness changes in hillslopes from Nahuelbuta are not further considered.

In the southern hemisphere the N-facing hillslope is expected to be slightly warmer (higher solar irradiation) and drier (due to higher evaporation) than the S-facing hillslope (e.g., Anderson et al., 2013). These differences in available soil moisture could potentially lead to different vegetation and soil thickness. In Pan de Azúcar, the soil thickness of the S- and N-facing mid-slope positions cannot be attributed to differences in vegetation cover because it is absent from both the N- and S-facing slopes. In Santa Gracia, however, the thicker soil in the S-facing mid-slope position than in N-facing position can either be attributed to higher vegetation cover in the S-facing position (e.g., Riebe et al., 2017) or subtle lithological changes (e.g. Oeser et al., 2018). Different vegetation on S-facing and N-facing slope positions in La Campana could explain the higher variability in soil thickness in the S-facing mid-slope positions (35 to 70 cm) than the N-facing hillslope (50 to 60 cm). However, the aspect-related differences in La Campana may represent local heterogeneities (e.g., physical erosion) rather than a hillslope aspect-related trend (Bernhard et al., 2018). Finally, in Nahuelbuta, the GPR envelopes indicate highly variable, but also slightly thicker soil thickness in the S-facing than the N-facing

https://doi.org/10.5194/soil-2020-33
Preprint. Discussion started: 15 June 2020

hillslopes. A higher clay content in the S-facing than the N-facing hillslope is attributed to a more intense soil formation in the S-facing hillslope (Bernhard et a., 2018). Differences in soil thickness on S- and N-facing hillslopes are increasing from N to S in latitude due to the increasing difference of solar irradiation on evaporation, vegetation, and possible frost cracking (e.g., Riebe et al., 2017).

Not only is there a change in soil thickness due to aspect, but also due to the latitude. Soil thickness increases and is more variable from N to S in latitude due to different climate and biota in each study area. Increasing precipitation rates from N to S allow an increase and diversity in vegetation. From N to S in latitude, soils increase in thickness and are more variable in thickness due to the influence of biota (e.g., trees, burrowing animals). The increase in biota not only causes variable soil thickness, but also homogenizes soils by bioturbation (e.g., Schaller et al., 2018). In addition, the increase in vegetation under increasing precipitation rates causes stabilization of hillslopes due to increasing precipitation rates (e.g., Langbein and Schumm, 1958; Starke et al., 2020). Hillslope denudation rates derived form *in situ*-produced cosmogenic nuclides increase from Pan de Azúcar to La Campana and slightly decrease for Nahuelbuta (Schaller et al., 2018; Oeser et al., 2018). Increasing soil thickness generally diminishes soil production rates (e.g., Heimsath et al., 1997) which under steady-state conditions equal hillslope denudation rates.

6 Conclusions

Soil thickness and properties are investigated in four study areas along a climate and vegetation gradient. The visually observed transition from mobile soil to immobile saprolite coincides with one or more changes in measured physical and chemical properties in each study area. These physical and chemical properties in turn, influence return-signals generated by Ground Penetrating Radar (GPR) in the sub-surface, but no systematic trend is visible for which physical or chemical properties correlate with GPR based observations of soil thickness. Given this, the measurements and interpretation of GPR signals for systematically identifying

https://doi.org/10.5194/soil-2020-33
Preprint. Discussion started: 15 June 2020

subsurface changes in physical and chemical properties is not straightforward and differs for each study area. In general, the better developed the soil the better the correlation of GPR signals from point locations with physical and chemical soil properties. We note that what frequency GPR antenna is best suited for identifying soil thickness is difficult, and calibration to local point locations (e.g. pedons) is always required. However, after local calibration between GPR signals and point locations is conducted, information of soil thickness from point locations can be up-scaled to hillslope transects with car

Acknowledgement

We would like to thank CONAF and all the Park Rangers for the possibility of working in the natural parks, for providing access to the sample locations, and help inside the National Parks. We acknowledge support from the German Science Foundation (DFG) priority research program SPP-1803 "EarthShape: Earth Surface Shaping by Biota" (sub grants KR 3725/1-1 and SCHA 1690/3-1). RD was supported by a DFG Emmy Noether grant (DR 822/3-1).

https://doi.org/10.5194/soil-2020-33
Preprint. Discussion started: 15 June 2020

References:

Abdi, H., and Williams, L.J. Principal component analysis, Wiley interdisciplinary reviews: computational statistics 2, 433-459, 2010.

Anderson, S.P., Anderson, S.P., and Tucker, G.E. Rock damage and regolith transport by frost: An example of climate modulation of the geomorphology of the critical zone, Earth Surface Processes and Landforms, DOI: 10.1002/esp.3330, 2013.

Aranha, P.R.A., Augustin, C.H.R.R., and Sobreira, F.G. The use of GPR for characterizing underground weathered profiles in the sub-humid tropics, Journal of Applied Geophysics, 49, 195-210, 2002.

Armesto, J.J., Vidiella, P.E., and Gutierrez, J.R. Plant communities of the fog-free coastal desert of Chile: plant strategies in a fluctuating environment, Revista Chilena de Historia Natural, 66, 271-282, 1993.

Bernhard, N., Moskwa, L.-M., Oeser, R., von Blanckenburg, F., Boy, H., Brucker, E., Dippold, M., Ehlers, T.A., Fuentes-Espoz J.P., Godoy, R., Köster, M., Osses, P., Paulino, L., Schaller, M., Scholten, T., Seguel, O., Spielvogel, S., Spohn, M., Stock, S., Stroncik, N., Uebernickel, K., Wagner, D., Kühn, P.: Pedogenic and microbial interrelations to regional climate and local topography: New insights from a climate gradient (arid to humid) along the Coastal Cordillera of Chile, Catena, 170, 335-355, 2018.

Birkeland, P.W. Soils and Geomorphology, Oxford University Press, New York, 1999.

Braun, J.-J., Descloitres, M., Riotte, J., Fleury, S., Barbiero, L., Boeglin, J.-L., Violette, A., Lacarce, E., Ruiz, L., Sekhar, M., Mohan Kumar, M.S., Subramanian, S., and Dupre, B. Regolith mass balance inferred from combined mineralogical, geochemical and geophysical studies: Mule Hole gneissic watershed, South India, Geochimica et Cosmochimica Acta, 73, 935-961, 2009.

Brimhall, G.H., and Dietrich, W.E. Constitutive mass balance relations between chemical composition, volume, density, porosity, and strain in metasomatic

https://doi.org/10.5194/soil-2020-33
Preprint. Discussion started: 15 June 2020

hydrochemical systems: Results on weathering and pedogenesis, Geochimica et Cosmochimica Acta, 51 (3), 567-587, 1987.

Brimhall, G.H., Alpers, C., and Cunningham, A.B. Analysis of supergene ore-forming processes using mass balance principles, Econoomic Geology, 80, 1227-1254, 1985.

Bro, R., and Smilde, A.K. Principal component analysis, Analytical Methods, 6, 2812-2831, 2014.

Chadwick, O.A., Brimhall, G.H., and Hendricks, D.M. From a black to a gray box - a mass balance interpretation of pedogenesis, Geomorphology, 3, 369-390, 1990.

Dal Bo, I., Klotzsche, A., Schaller, M., Ehlers, A.T., Kaufmann, M.S., Fuentes-Espoz, J.P., Vereecken, H., van der Kruk, J. Geophysical imaging of regolith in landscapes along a climate and vegetation gradient in the Chilean Coastal Cordillera, Catena, 180, 146-159, 2019.

De Coster, A., and Lambot, S. Fusion of Multifrequency GPR Data Freed From Antenna Effects, Journal of Selected Topics in Applied Earth Observations and Remote Sensing, 11 (2),.664-674, 2018.

Doolittle, J.A., and Collins, M.E. Use of soil information to determine application of ground penetrating radar. Journal of Applied Geuphysics, 33 (1-3), 101-105, 1995.

Doolittle, J.A., Minzenmayer, F.E., Waltman, F.W., Benham, E.C., Tuttle, J.W., and Peaslee, S.D. Ground-penetrating radar soil suitability map of the conterminous United States, Geoderma, 141, 416-421, 2007.

Gerber, R., Felix-Henningsen, P., Behrens, T., and Scholten, T. Applicability of ground-penetrating rader as a tool for nondestructive soil-depth mapping on Pleistocene slope deposits, Journal of Plant Nutrition and Soil Science, 173 (2), 173-184, 2010.

Green, A.G. Applications of 3-D georadar methods to diverse environmental and engineering problems, Progress in Environmental and Engineering Geophysics, edited by Chao, C. and Jianghai, X., Science Press USA, 220-226, 2004.

https://doi.org/10.5194/soil-2020-33
Preprint. Discussion started: 15 June 2020

Guo, L., Chen, J., Cui, X., Fan, B., and Lin, H. Application of ~~graound~~ penetrating radar for coarse root detection and quantification: a review, Plant Soil, 362, 1-23, 2013.

Guo, L., Mount, G.J, Hudson, S., Lin, H., and Levia, D. Pairing ~~geohpysical~~ techniques helps understanding of the near-~~surfce~~ Critical Zone: Visualization of preferential ~~rouging~~ of stemflow along coarse roots. Geoderma, 357, 113953, 2020.

Heimsath, A.M., Dietrich, W.E., Nishiizumi, K., and Finkel, R.C. The soil ~~productionfunction~~ and landscape equilibtium, Nature, 388, 358-361, 1997.

Heimsath, A.M., Dietrich, W.E., Nishiizumi, K., and Finkel, R.C. Cosmogenic nuclides, topography, and the spatial variation of soil depth, Geomorphology, 27, 151-172, 1999.

Hilgard, E.W. Soils: Their Formation, Properties, Compositions and Relations to Climate and Plant Growth in the Humid and Arid Regions, The Macmillan Company, New York, 1914.

Holbrook, W.S., Riebe, C.S., Elwaseif, M., Hayes, J.L., Vasler-Reeder, K., Harry, D.L., Malazian, A., Dosseto, A., Hartsough, P.C., and Hopmans, W. Geophysical constraints on deep weathering and water storage potential in the Southern Sierra Critical Zone Observatory. Earth Surface Processes and Landforms, 39, 366-380, 2014.

Hruska, J., Cermak, J., and Sustek, S. Mapping tree root system with ground-penetrating radar. Tree Physiology, 19, 125-130, 1999.

Jenny, H. Factors of Soil Formation: A System of Quantitative Pedology, Dover Publications, New York, 1994.

Jol, H.M. (Ed.): Ground penetrating radar: theory and applications, Elsevier Science, Amsterdam, the Netherlands ; Oxford, United Kingdom, 2009.

Kassambara, A. Practical guide to cluster analysis in R: unsupervised machine learning, STHDA, 2017.

Langbein, W.B., and Schumm, S.A. Yield of sediment in relation to mean annual precipitation, Transaction American Geophysical Union, 39, 1076-1084, 1958.

Liu, J.L., and Marfurt, K.J. Instantaneous Spectral Attributes to Detect Channels, Geophysics, 72, 23-31. http://dx.doi.org/10.1190/1.2428268, 2007.

Mellett, J.S. Ground penetrating radar applications in ~~engeneering~~, environmental management, and geology, Journal of Applied Geophysics, 33 (1-3), 157-166, 1995.

Miller, T.W., Hendrickx, J.M.H., and Borchers, B. Radar detection of ~~burried~~ landmines field soils. Vadose Zone Journal, 3 (4). 1116-1127, 2002.

Mutz, S.G., Ehlers, T.A., Werner, M., Lehmann, G., Stepanek, C., and Li, J. Where is Late Cencozoic climate change most likely to impact denudation?, Earth Surface Dynamics, 6, 271-301, https://doi.org/10.5194/esurf-2017-47, 2018.

Oeser, R.A., Stroncik, N., Moskwa, L.-M., Bernhard, N., Schaller, M., Canessa, R., van der B Rin, L., Köster, M., Brucker, E., Stock, SS., Fuentes, J..P., Godoy, R., Matus., F.J., Oses Pedraza, R., Osses McIntyre, P., Paulino, L., Seguel, O., Bader, M.Y., Boy, J., Dippold, M.A., Ehlers, T.a., Kühn, P., Kuzyakiv, Y., Peinweber, P., Scholten, T., Spielvogel, S., Spohn, M., Üubernickel, K., Tielbörger, K., Wagner, D., and von Blanckenburg, F. Chemistry and microbiology of the Critical Zone along a steep climate and vegetation gradient in the Chilean Coastal Cordillera, Ctena, 170, 183-203, 2018.

Parsekian, A.D., Singha, K., Minsley, B.J., Holbrook, W.S., and Slater, L. Multiscale geophysical imaging of the critical zone, Reviews of Geophysics, 53, 1-26, 2015.

Porder, S., Vitousek, M.P., Chadwick, O.A., Chamberlain, C. P. and Hilley, G.E. Uplift, Erosion, and Phosphorous Limitation in Terrestrial Ecosystems, Ecosystems, 10, 158-170, 2007.

Rabassa, J., and Clapperton, C.M. Quaternary glaciations of the southern Andes, Quaternary Science Reviews, 9, 153-174, 1990.

Riebe, C.S., and Granger, D. Quantifying deep and near-surface chemical erosion on cosmogenic nuclides in soils, saprolite, and sediment, Earth Surface Processes and Landforms, 38, 523-533, 2013.

https://doi.org/10.5194/soil-2020-33
Preprint. Discussion started: 15 June 2020

Riebe, C.S., Hahm, W.J. and Brantley, S.L. Controls on deep critical zone architecture: a historical review and four testable hypothesis, Earth Surface Processes and Landforms, 42, 128-156, 2017.

Roering, J.J., Kirchner, J.W., and Dietrich, W.E. Hillslope evolution by nonlinear, slope-dependent transport: Steady state morphology and equilibrium adjustment timescales, Journal of Geophysical Research, 106, B8, 16499-16513. 2001.

Roering, J.J., Marshall, J., Booth, A.M., Mort, M., and Jin, Q. Evidence for biotic controls on topography and soil production, Earth and Planteray Science Letters, 289, 183-190, 2010.

Saarenketo, T. Electrical properties of water in clay and silty soils. Journal of Applied Geophysics, 40, 73-88, 1998.

Sarkar, R., Paul, K.B., and Higgins, T.R. Impacts of soil physiochemical properties and temporal-seasonal soil-environmental status on ground-penetrating radar response. Soil Science Society of America Journal, 83, 542-554, 2019.

Scarpone, C., Schmidt, M.G., Bulmer, C.E., and Knudby, A. Modelling soil thickness in the critical zone for Southern British Columbia, Geoderma, 282, 59–69, 2016.

Schaller, M., Ehlers, T., Lang, K., Schmid, M., and Fuentes-Espoz, J. Addressing the contribution of climate and vegetation cover on hillslope denudation, Chilean Coastal Cordillera (26°–38° S), Earth and Planetary Science Letters, 489, 111-122, 2018.

Sedgwick, P. Pearson's correlation coefficient, BMJ, 345:e4483, 2012.

Starke, J., Ehlers, T.A., and Schaller, M. Latitudinal effect of vegetation on erosion rates identified along western South America. Science, 367, 1358-1361, 2020.

Sucre, E.B., Tuttle, J.W., and Fox, T.R. The use of ground-penetrating radar to accurately estimate soil depth in rocky forest soils. Forest Science 57 (1), 59-66, 2011.

Telford, W.M., Geldart, L.P., Sheriff, R.E. and Keys, D.A. (Eds.): Applied Geophysics, 2th Edition, Cambridge University Press, Cambridge, 770. http://dx.doi.org/10.1017/CBO9781139167932, 1990.

Tosti, F., Patriarca, C., Slob, E., Benedetto, A., and Lambot, S. Clay content evaluation in soils through GPR signal processing. Journal of Applied Geohpysics, 97, 69-80, 2013.

Wei, T. Package 'corrplot'-Visualization of a correlation matrix. v0.60. cran. rproject. org, 2012.

Werner, C., Schmid, M., Ehelrs, T.A., Fuentes-Espoz, J.P., Steinkamp, J., Forrest, M., Liakka, J., Maldonado, A., and Hickler, T. Effect of changing vegetation and precipitation on denudation - Part1; Predicted vegetation composition and cover over the last 21 thousand years along the Coastal Cordillera of Chile, Earth Surface Dynamics, 6, 829-858, https://doi.org/10.5194/esurf-6-829-2018, 2018.

Wold, S., Esbensen, K., and Geladi, P. Principal component analysis, Chemometrics and intelligent laboratory systems, 2, 37-52, 1987.

Zhang, J., Lin, H., and Doolittle, J. Soil layering and preferential flow impacts on seasonal changes of GPR signals in two contrasting soils. geoderman, 213, 560-569, 2014.

Figure captions

Fig. 1:

Digital elevation model (Data source: GTOPO30) for the Chilean Coastal Cordillera and the Central Andes showing the four investigated study areas (from N to S): Pan de Azúcar (~26° S); Santa Gracia (~30° S); La Campana (~33° S); and Nahuelbuta (~38° S).

Fig. 2:

Satellite images (Data source: Google Earth©) of the four study areas from N to S in latitude: A) Pan de Azúcar; B) Santa Gracia; C) La Campana; and D) Nahuelbuta. Red stars indicate the pedon positions whereas the blue lines represent the locations of the geophysical investigations.

https://doi.org/10.5194/soil-2020-33
Preprint. Discussion started: 15 June 2020

Fig. 3:

N- and S-facing hillslopes of the four study areas with locations of soil pedons and transects of ground penetrating radar indicated by the red double arrows.

Fig. 4:

Compilation of physical and chemical investigations with depth at the pedon location in the mid-slope position of the S-facing hillslope in Pan de Azúcar. Properties shown are: 1) GPR transect and the envelope profile of the 500 MHz measurement; 2) GPR transect and the envelope profile of the 1000 MHz measurement; 3) Bulk density; 4) Grain size distribution of sand, silt, and clay; 5) Loss on ignition LOI; 6) Chemical index of alteration CIA 7) Chemical index of the mass transfer coefficient Tau τ; and 8) volumetric strain ε_{strain}. The black line indicates the boundary between the mobile soil and the immobile saprolite (after Oeser et al., 2018) and the gray area with green lines reflects the transition zone from B to C horizon (after Bernhard et al., 2018).

Fig. 5:

Primary component analysis PCA of properties for all four soil pedons in Pan de Azúcar. A) Scree plot showing the percentage of explained variances and B) Variables - PCA.

Fig. 6:

Compilation of physical and chemical investigations at the pedon location in the mid-slope position of the S-facing hillslope in Santa Gracia. Properties shown are listed in caption of Fig. 4.

Fig. 7:

Primary component analysis PCA of properties for all four soil pedons in Santa Gracia.

https://doi.org/10.5194/soil-2020-33
Preprint. Discussion started: 15 June 2020

Fig. 8:
Compilation of physical and chemical investigations at the pedon location in the mid-slope position of the S-facing hillslope in La Campana. Properties shown are listed in in caption of Fig. 4.

Fig. 9:
Primary component analysis PCA of properties for all four soil pedons in La Campana.

Fig. 10
Compilation of physical and chemical investigations at the pedon location in the mid-slope position of the S-facing hillslope in Nahuelbuta. Properties shown are listed as in caption of Fig. 4. Note that only the 500 MHz signal and envelope profile exist.

Fig. 11:
Primary component analysis PCA of properties for all four soil pedons in Nahuelbuta.

Fig. 12:
A) 1000 MHz GPR transect and B) envelope for the S-facing hillslope in Pan de Azúcar. The hillslope transect spans over ~20 m and includes pedon AZPED60, AZPED50, and AZPED40 (black boxes). The potential soil thickness based on the envelopes is indicated by stars (in B). The red bar indicates the B to C horizon transition as given in Bernhard et al. (2018). Uphill is from left to right. Note that in the radar data the air wave and background removal is applied.

Fig. 13:
1000 MHz GPR signal and envelope for the mid-slope position of the S-facing hillslope position in Santa Gracia (SGPED40). The hillslope transect spans over ~20

https://doi.org/10.5194/soil-2020-33
Preprint. Discussion started: 15 June 2020

m. Interpretation of the radar signal are indicated where possible (stippled lines in A and B). The potential soil thickness is indicated based on the envelope profile. Uphill is from left to right. Lines and symbols in figures as described in Fig. 12.

Fig. 14:
500 MHz GPR signal and envelope for the mid-slope position of the S-facing hillslope in La Campana (LCPED20). The hillslope transect spans over ~8 m. Interpretation of the radar signal are indicated where possible (stippled and black lines in A and B). The potential soil thickness is indicated based on the envelope profile. Uphill is from left to right. Lines and symbols in figures as described in Fig. 12.

Fig. 15:
500 MHz GPR signal and envelope for the mid-slope position of the S-facing hillslope in Nahuelbuta (NAPED20). The hillslope transect spans over ~20 m. Interpretation of the radar signal are indicated where possible (stippled lines in A and B). The potential soil thickness is indicated based on the envelope profile. Uphill is from left to right. Lines and symbols in figures as described in Fig. 12.

https://doi.org/10.5194/soil-2020-33
Preprint. Discussion started: 15 June 2020

Fig. 1:

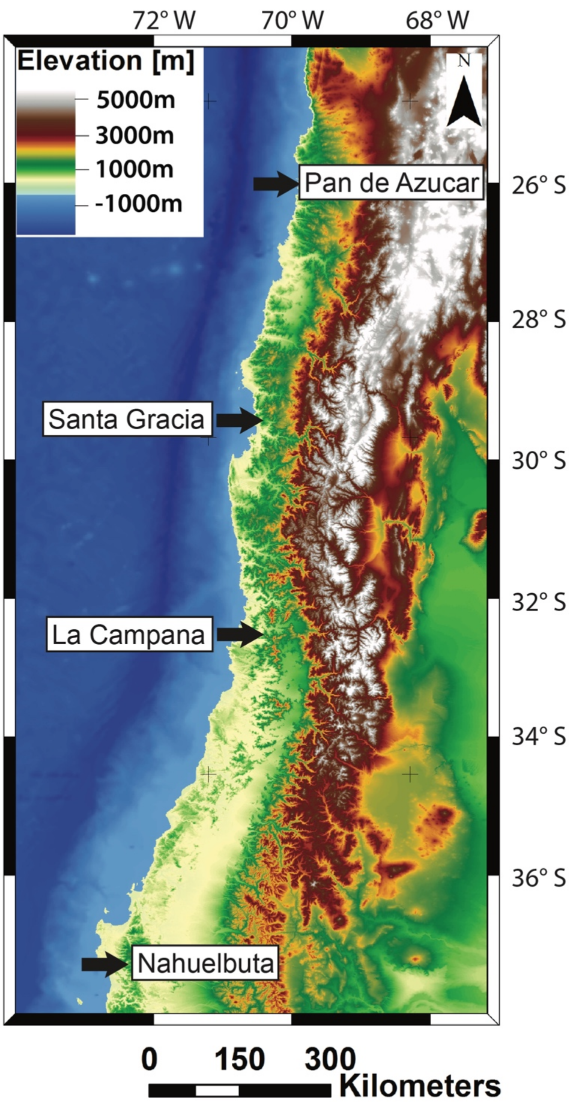

https://doi.org/10.5194/soil-2020-33
Preprint. Discussion started: 15 June 2020

949 Fig. 2:

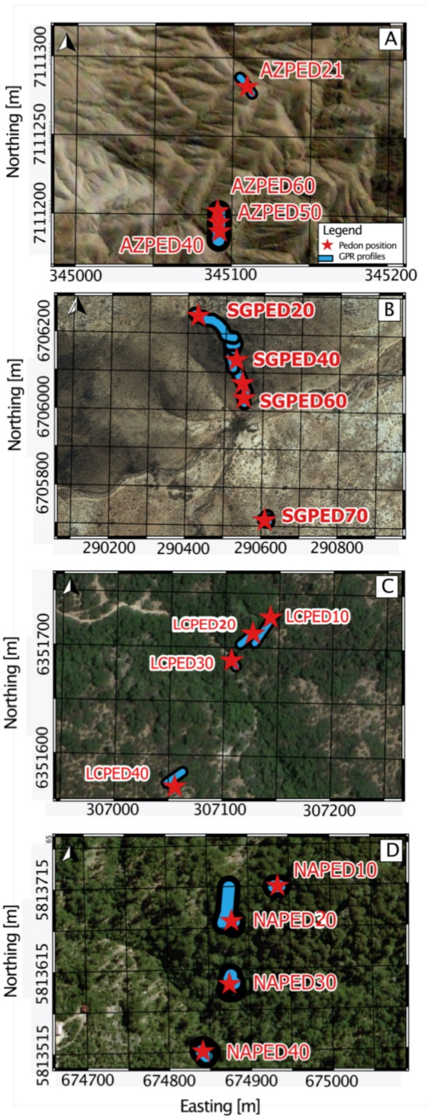

950

https://doi.org/10.5194/soil-2020-33
Preprint. Discussion started: 15 June 2020

Fig. 3:

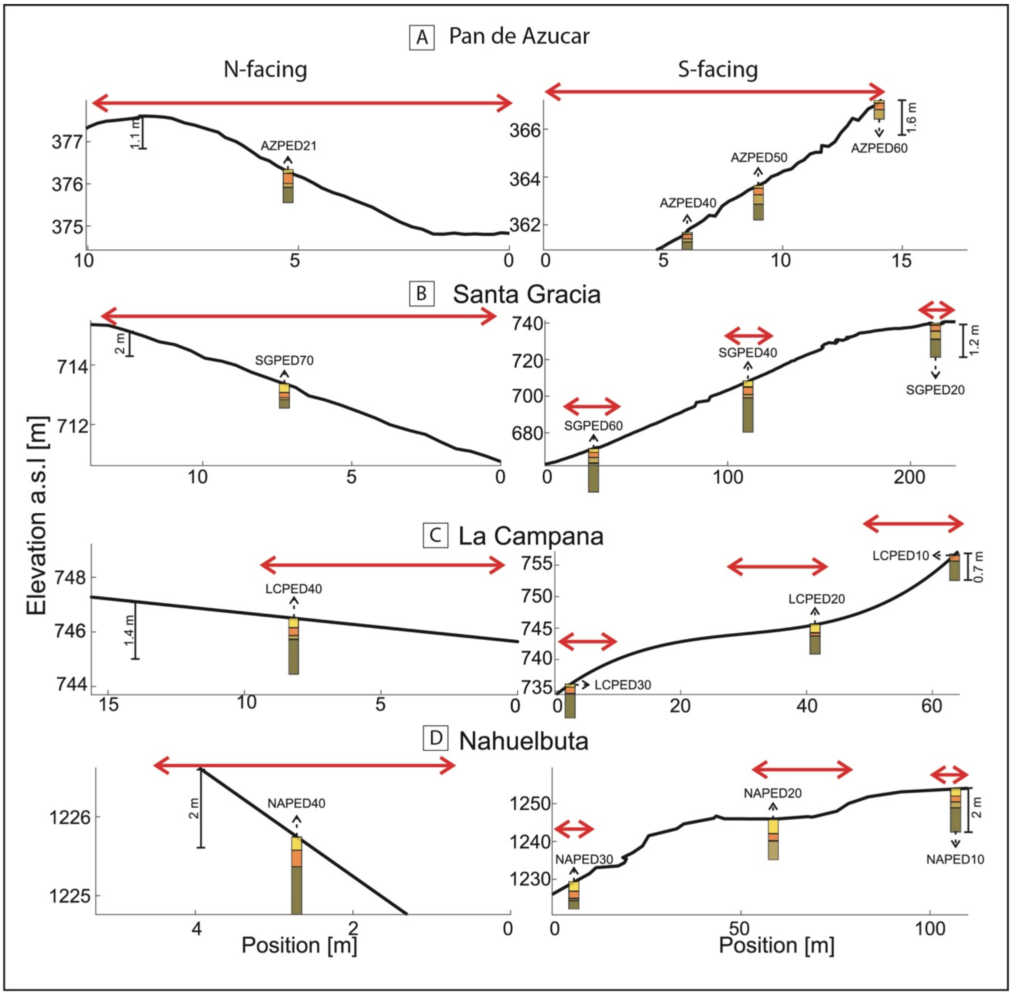

https://doi.org/10.5194/soil-2020-33
Preprint. Discussion started: 15 June 2020

Fig. 4:

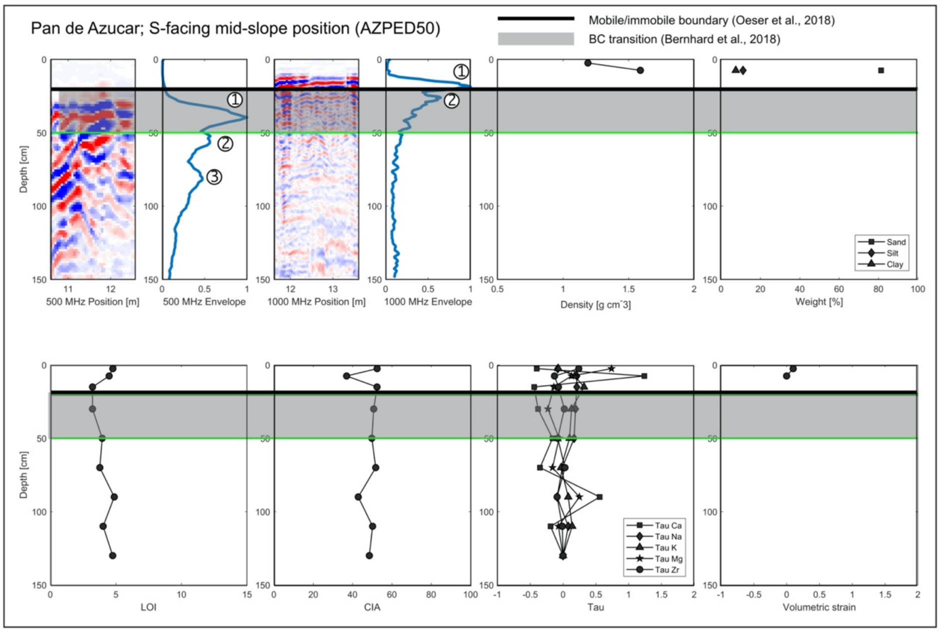

Fig. 5:

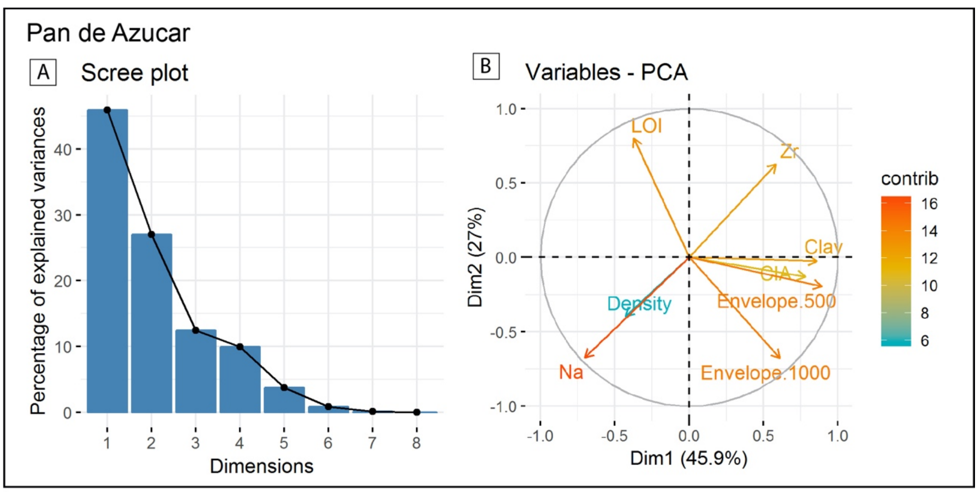

https://doi.org/10.5194/soil-2020-33
Preprint. Discussion started: 15 June 2020

Fig. 6:

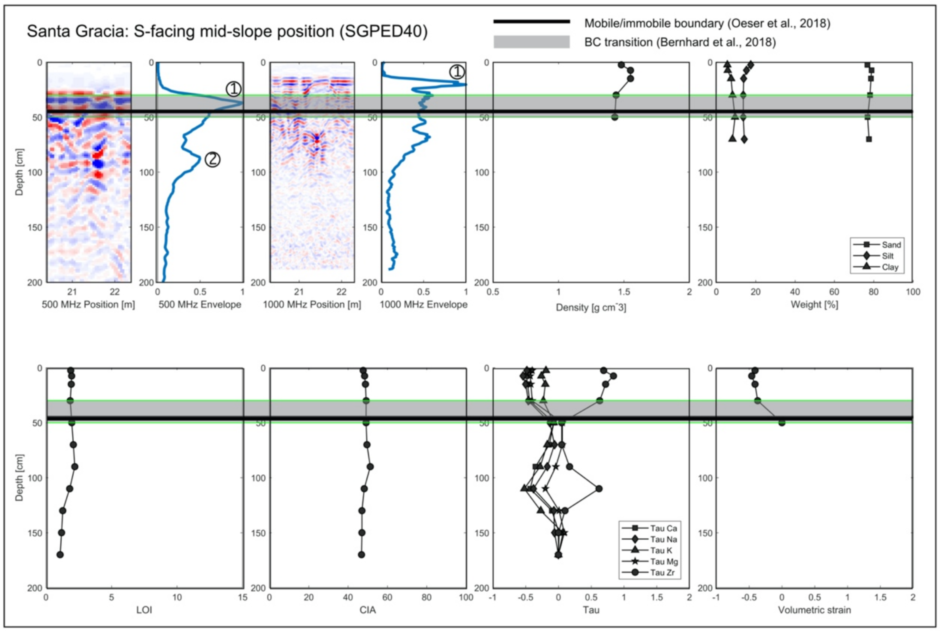

Fig. 7:

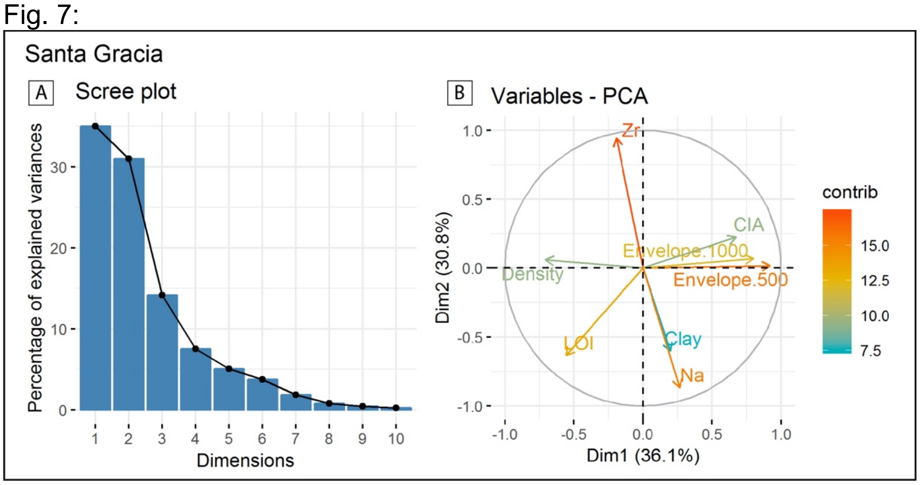

https://doi.org/10.5194/soil-2020-33
Preprint. Discussion started: 15 June 2020

Fig. 8:

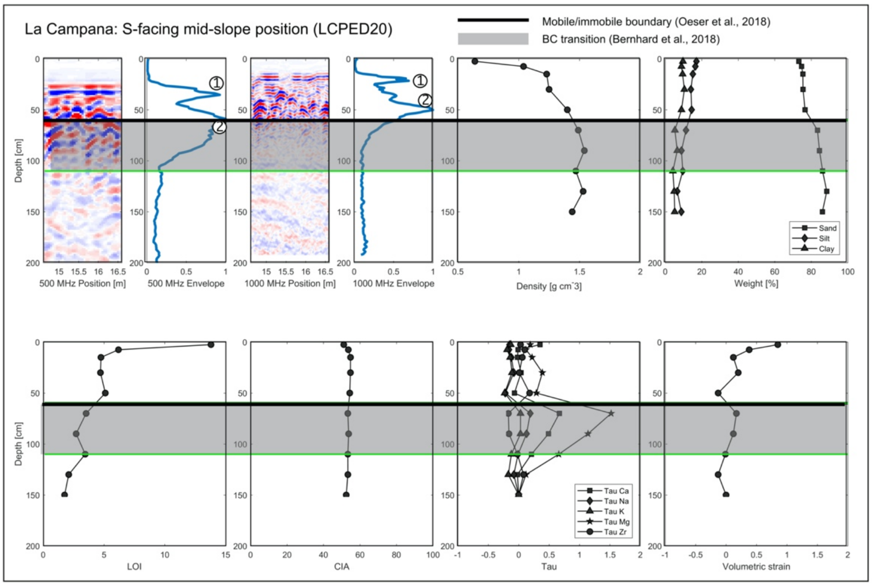

Fig. 9:

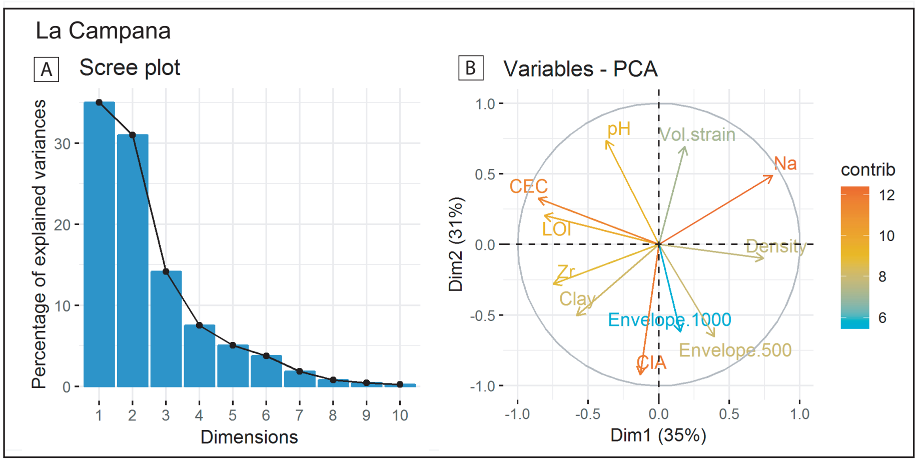

https://doi.org/10.5194/soil-2020-33
Preprint. Discussion started: 15 June 2020

Fig. 10:

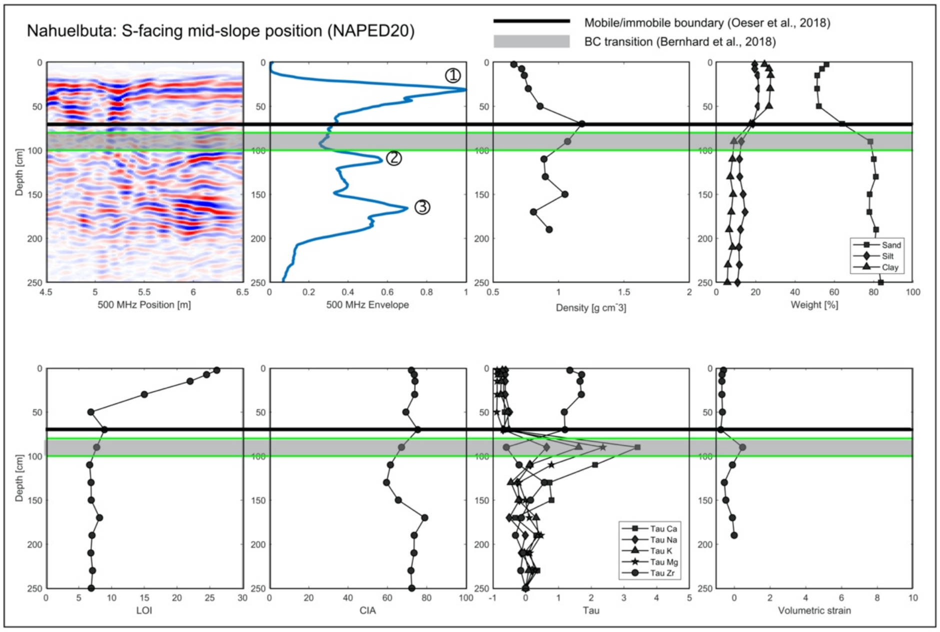

Fig. 11:

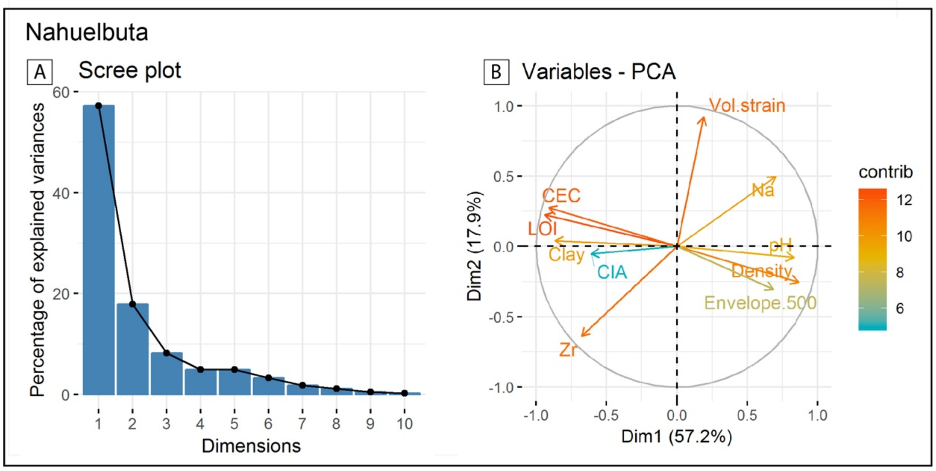

https://doi.org/10.5194/soil-2020-33
Preprint. Discussion started: 15 June 2020

Fig. 12:

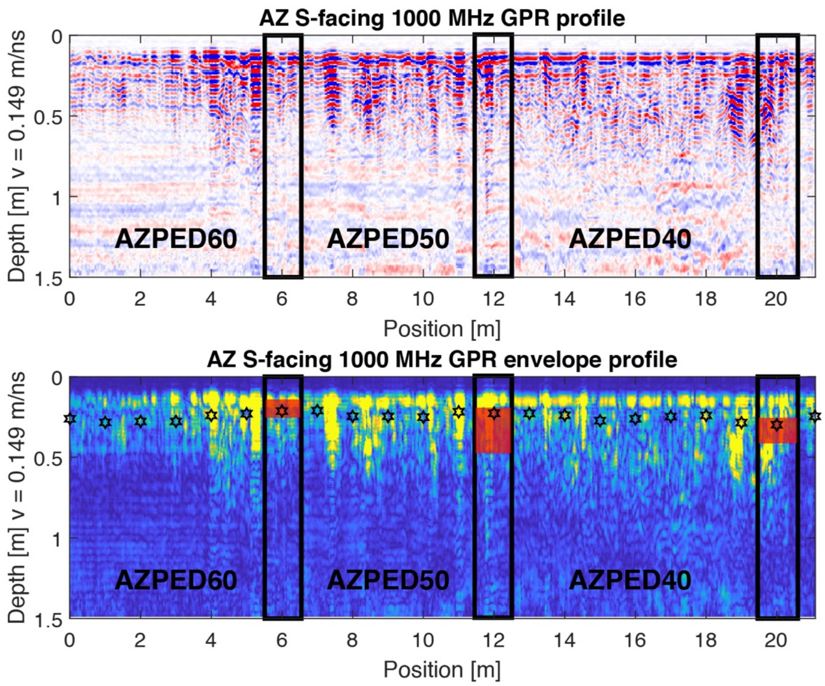

https://doi.org/10.5194/soil-2020-33
Preprint. Discussion started: 15 June 2020

Fig. 13:

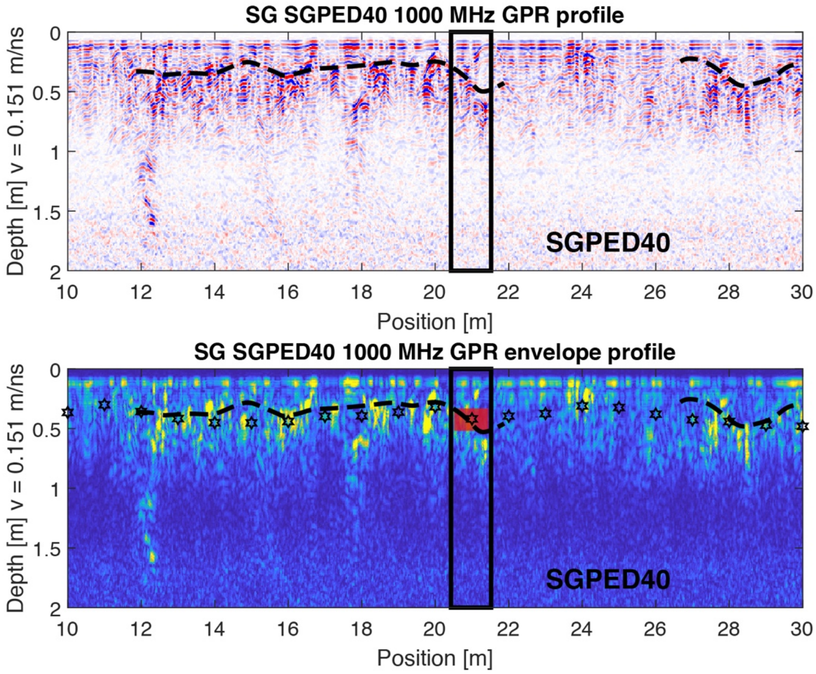

https://doi.org/10.5194/soil-2020-33
Preprint. Discussion started: 15 June 2020

Fig. 14:

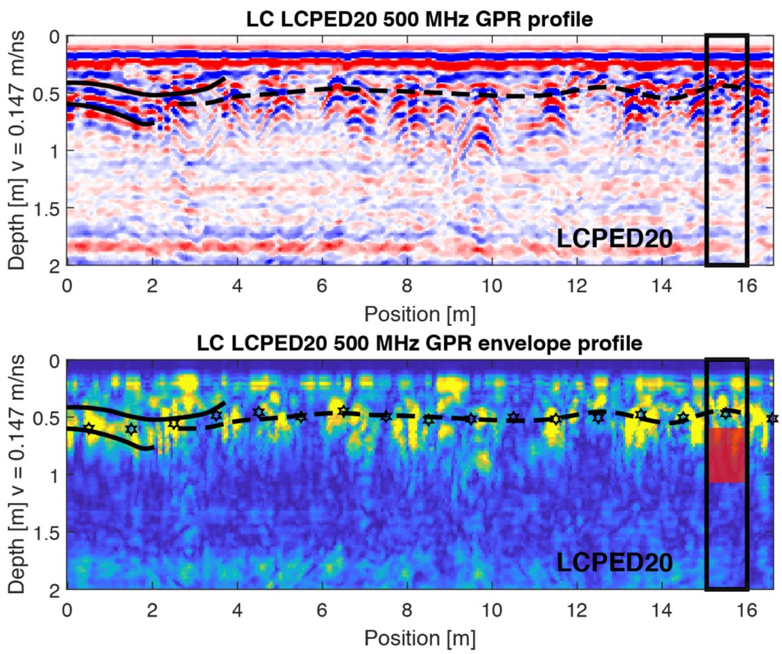

https://doi.org/10.5194/soil-2020-33
Preprint. Discussion started: 15 June 2020

Fig. 15:

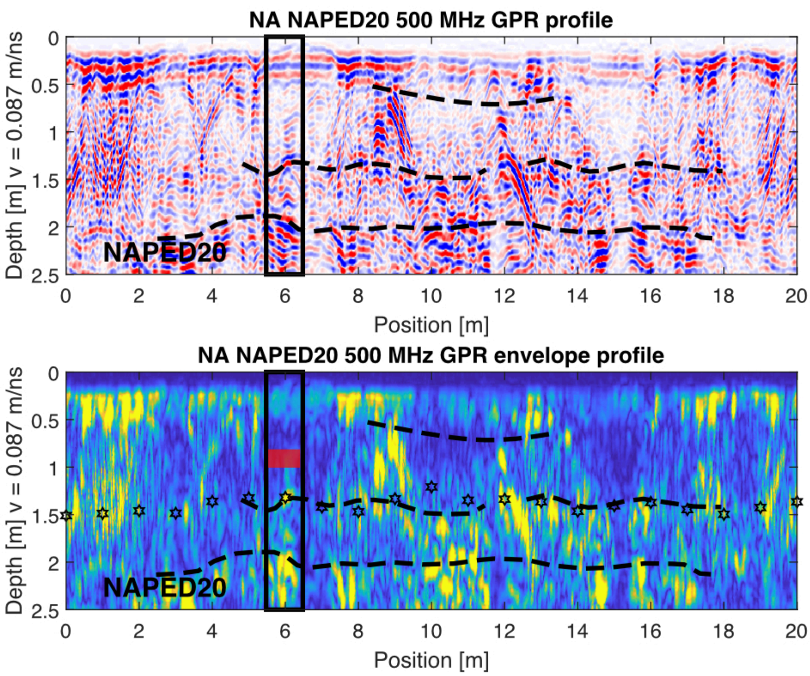

Table 1:

Table 1: Overview of physical, chemical, and geohpysical properties determined in the four different study areas				
Property	Abreviation	Units	Meaning	Reference
Soil bulk density	ρb	g/cm^3	Weight of unit volume	Bernhard et al., 2018
Grain size distributioin	GSD	%	Weight percent of different grain sizes smaller than 2 mm	Bernhard et al., 2018
Potential hydrogene	pH		Acid and base properties	Bernhard et al., 2018
Cation exchange capacity	CEC	$cmol_c/kg$	Soil ability to hold positively charged ions	Bernhard et al., 2018
Loss on ignition	LOI	%	Loss of volatiles due to excessiv heating	Oeser et al., 2018
Chemical index of alteration	CIA		Degree of weathering	Oeser et al., 2018
Mass trasnfer coefficient	τ	m/s	Chemical gain or loss	Oeser et al., 2018
Volumetric strain	ε_{strain}		Volumetric grain or loss	Oeser et al., 2018
Electric permitivity	ε_r		Structural changes, porosity/soil water content	Dal Bo et al., 2019; This study
Electrical conductivity	σ	mS/m	Clay, salinity	Dal Bo et al., 2019; This study

Table 2:

Table 2: Data compilation for pedons in the investigated four study areas in the Chilean Coastal Cordillera

Soil profile	Location		Altitude	Position	Aspect	Slope	Field observations: BC-horizon transition[1]	Field observations: Mobile/immob.[2]	Field observations: Mobile/immob.[3]	GPR[4]	GPR point depth[5]: 500 MHz	GPR point depth[5]: 1000 MHz	GPR transect depth[6]: 500 MHz	GPR transect depth[6]: 1000 MHz
	°S	°W	m		°	°	cm	cm	cm	cm	cm	cm	cm	cm
Pan de Azucar														
AZPED60	26.11012	70.54922	343	top	60	5	14-26		22	30-55 (?)	40	20/25/45		
AZPED50	26.11027	70.54922	333	mid	0	40	20-50	20	20	20-55	40/50/70	20/25/35/45	36 ± 1	25 ± 3
AZPED40	26.11024	70.54921	326	toe	0	33	23-40		25	20-40	40/55	20/30		
AZPED21	26.10936	70.54907	342	mid	180	25	20-30	20	20	30-45	37/55/75	20/30/45/55	40 ± 2	28 ± 7
Santa Gracia														
SGPED20	29.75636	71.16721	718	top	240	5	20-30		30	30	40	20/30/40/50	37 ± 5	34 ± 3
SGPED40	29.75738	71.16635	682	mid	0	25	30-50	50	45	60	45	20/30/40/55/65	40 ± 7	36 ± 5
SGPED60	29.75826	71.16615	638	toe	0	20	40-60		55	-	37/50	20/30	39 ± 7	35 ± 6
SGPED70	29.76120	71.16559	690	mid	180	15	25	35	35	NA	40	20/30	35 ± 3	28 ± 2
La Campana														
LCPED10	32.95581	71.06332	734	top	60	7	34		45	40/50	35/50/70	20/30/35/50/65	55 ± 6	44 ± 5
LCPED20	32.95588	71.06355	718	mid	0	23	60-110	60	60	50/60	35/60/70	20/38/50	59 ± 6	45 ± 4
LCPED30	32.95615	71.06380	708	toe	60	35	34-55		55	45/50	35/70	20/30/38	50 ± 9	41 ± 4
LCPED40	32.95720	71.06425	724	mid	120	12	36-103	35	35	-	35/65	20/30/40	56 ± 6	47 ± 6
Nahuelbuta														
NAPED10	37.80735	73.01285	1248	top	60	5	50-75		70	70/75	35/45/120		82 ± 15	
NAPED20	37.80770	73.01357	1239	mid	60	15	80-100	95	70	75/95	35/110/170		101 ± 8	
NAPED30	37.80838	73.01345	1228	toe	0	20	63-85		90	-	5/90/120/140		96 ± 6	
NAPED40	37.80904	73.01380	1200	mid	180	13	65-90	70	60	40/50	40/80/120		95 ± 11	

[1] Depth of BC-horizon transition from Bernhard et al., 2018
[2] Depth of mobile layer from Schaller et al., 2018
[1] Depth of mobile layer from Oeser et al., 2018
[4] Depth based on data from Dal Bo et al., 2019
[5] Depth based on single point GPR envelopes (This study)
[6] Average depth based on envelopes from GPR transect data (This study)